

Journal of Biomedical Optics

SPIEDigitalLibrary.org/jbo

Imaging-guided two-photon excitation-emission-matrix measurements of human skin tissues

Yingqiu Yu
Anthony M. D. Lee
Hequn Wang
Shuo Tang
Jianhua Zhao
Harvey Lui
Haishan Zeng

Imaging-guided two-photon excitation-emission-matrix measurements of human skin tissues

Yingqiu Yu,^{a,b} Anthony M. D. Lee,^a Hequn Wang,^a Shuo Tang,^b Jianhua Zhao,^{a,c} Harvey Lui,^{a,c} and Haishan Zeng^{a,c}

^aImaging Unit, Integrative Oncology Department, British Columbia Cancer Agency Research Center, 675 West 10th Avenue, Vancouver, BC, V5Z 1L3, Canada

^bUniversity of British Columbia, Department of Electrical and Computer Engineering, 5500-2332 Main Mall, Vancouver, BC, V6T 1Z4, Canada

^cUniversity of British Columbia and Vancouver Coastal Health Research Institute, Department of Dermatology and Skin Science, 835 West 10th Avenue, Vancouver, BC, V5Z 4E8, Canada

Abstract. There are increased interests on using multiphoton imaging and spectroscopy for skin tissue characterization and diagnosis. However, most studies have been done with just a few excitation wavelengths. Our objective is to perform a systematic study of the two-photon fluorescence (TPF) properties of skin fluorophores, normal skin, and diseased skin tissues. A nonlinear excitation-emission-matrix (EEM) spectroscopy system with multiphoton imaging guidance was constructed. A tunable femtosecond laser was used to vary excitation wavelengths from 730 to 920 nm for EEM data acquisition. EEM measurements were performed on excised fresh normal skin tissues, seborrheic keratosis tissue samples, and skin fluorophores including: NADH, FAD, keratin, melanin, collagen, and elastin. We found that in the stratum corneum and upper epidermis of normal skin, the cells have large sizes and the TPF originates from keratin. In the lower epidermis, cells are smaller and TPF is dominated by NADH contributions. In the dermis, TPF is dominated by elastin components. The depth resolved EEM measurements also demonstrated that keratin structure has intruded into the middle sublayers of the epidermal part of the seborrheic keratosis lesion. These results suggest that the imaging guided TPF EEM spectroscopy provides useful information for the development of multiphoton clinical devices for skin disease diagnosis. © 2012 Society of Photo-Optical Instrumentation Engineers (SPIE). [DOI: 10.1117/1.JBO.17.7.077004]

Keywords: two-photon excitation fluorescence; second harmonic generation; two-photon excitation fluorescence excitation-emission matrix; multiphoton imaging; skin fluorophore; seborrheic keratosis.

Paper 12189 received Mar. 21, 2012; revised manuscript received May 23, 2012; accepted for publication May 30, 2012; published online Jul. 6, 2012.

1 Introduction

As skin cancer is the most prevalent type of cancer, it is important to develop diagnostic techniques for accurate early stage diagnosis to improve the chances for curative action. Nonlinear optical imaging methods are very promising for noninvasive diagnosis of skin diseases, leveraging the advantages of deep imaging depth, high resolution, fast imaging speed, and rich endogenous fluorophores.¹ Two nonlinear imaging mechanisms, two-photon excited fluorescence (TPF) and second harmonic generation (SHG) have been widely applied in research for skin characterization and diagnosis.²⁻⁴ Because different endogenous fluorophores can generate comparable intensities of TPF, integrated TPF imaging alone may not be sufficient to provide biochemical composition information. However, TPF spectral measurements can provide biochemical and constituent information of the tissue, and it can be sensitive to the physiological state of the skin and the presence of disease. Several groups have used TPF spectroscopic analysis for *in vivo* or *ex vivo* tissue studies at one or a few excitation wavelengths.⁵⁻⁸ Collection of the TPF emission spectrum as a function of excitation wavelength to generate a two-photon excitation-emission matrix (2P-EEM) can allow even greater sensitivity to distinguish fluorophores and disease states. EEM can also assist in choosing the optimal excitation/

emission wavelengths for the best performance of imaging analysis of specific tissue types. EEM of purified fluorophore may serve as a unique signature. Based on these signatures, EEM of complex tissues can be used to identify the fluorophores and their relative distributions in the tissue in a more reliable manner. The variations of emission from intrinsic fluorophores with the change of excitation wavelengths can be used to analyze the biochemical state of cells and tissues. EEM can display these variations within a single contour plot and thus facilitate fast and reliable analysis.

One-photon EEM has been widely investigated for skin research,⁹ and research has also shown the difference between one-photon spectra and two-photon spectra.⁸ When conventional single-photon EEM is applied to bulk tissue, the result is a mixture of signals emitted from different tissue depths, which is hard to interpret for analysis of tissue compositions. In two-photon EEM study, using the optical sectioning capability of TPF and SHG, EEM can be acquired from a specific thin layer and even a specific small region-of-interest. Spectral analysis can then be accurately targeted to particular locations in skin tissues with minimal interference from the surrounding tissues. Furthermore, SHG is a new contrast in two-photon EEM, which can provide extra information of collagen fibers in skin dermis. Moreover, two-photon emissions (TPF and SHG) in the UV-visible range are excited by a laser beam in the near IR range. Hence the excitation beam will incur less absorption

Address all correspondence to: Haishan Zeng, Imaging Unit, Integrative Oncology Department, British Columbia Cancer Agency Research Centre, 675 West 10th Ave, Vancouver, BC, Canada V5Z 1L3. Tel: 604 675 8083; Fax: 604675 8099; E-mail: hzen@bccrc.ca

tubes (PMT) for TPF and SHG imaging, respectively. Emission spectra are collected by a spectrometer (SpectraPro-150, Roper Scientific, Princeton, NJ) for EEM data accumulation. The exposure time for each emission spectrum was between 2 and 3 s. During this time period, the laser beam had scanned over the ROI for 24 to 36 times. Therefore, each emission spectrum represented the average emission signal (SHG or TPF) from the ROI. A specially designed fiber bundle was applied here to increase the collection area of emitted photons for a high signal-to-noise ratio in the spectral acquisition. The arrangement of fibers within the fiber bundle between the imaging system and the spectrometer has two different patterns (Fig. 1, inset a and inset b). The fiber bundle has 90 small fibers [single fiber core diameter: 100 μm ; numerical aperture (NA):

0.12] arranged in a hexagon pattern at the input end to provide a much larger collection area than a single fiber. The output end (Fig. 1, inset b) has all of the 90 fibers arranged as 2 straight lines with 45 fibers in each line so that most of the collected light can be coupled into the narrow entrance slit of the spectrometer. The width of this line-shape bundle of fibers is 200 μm , leading to a spectral resolution of 4 nm. The f -number ($f/\#$) of the spectrograph system ($f/4$) has been matched with the NA of the fiber (0.12) as: $f/\# = 1/(2 \times \text{NA})$ for optimum performance. (Fig. 1).

Due to the sinusoidal scanning pattern of the resonant scanner, a linearization algorithm was applied to correct the resulted image distortion,¹² which was incorporated into the system software for real-time display.

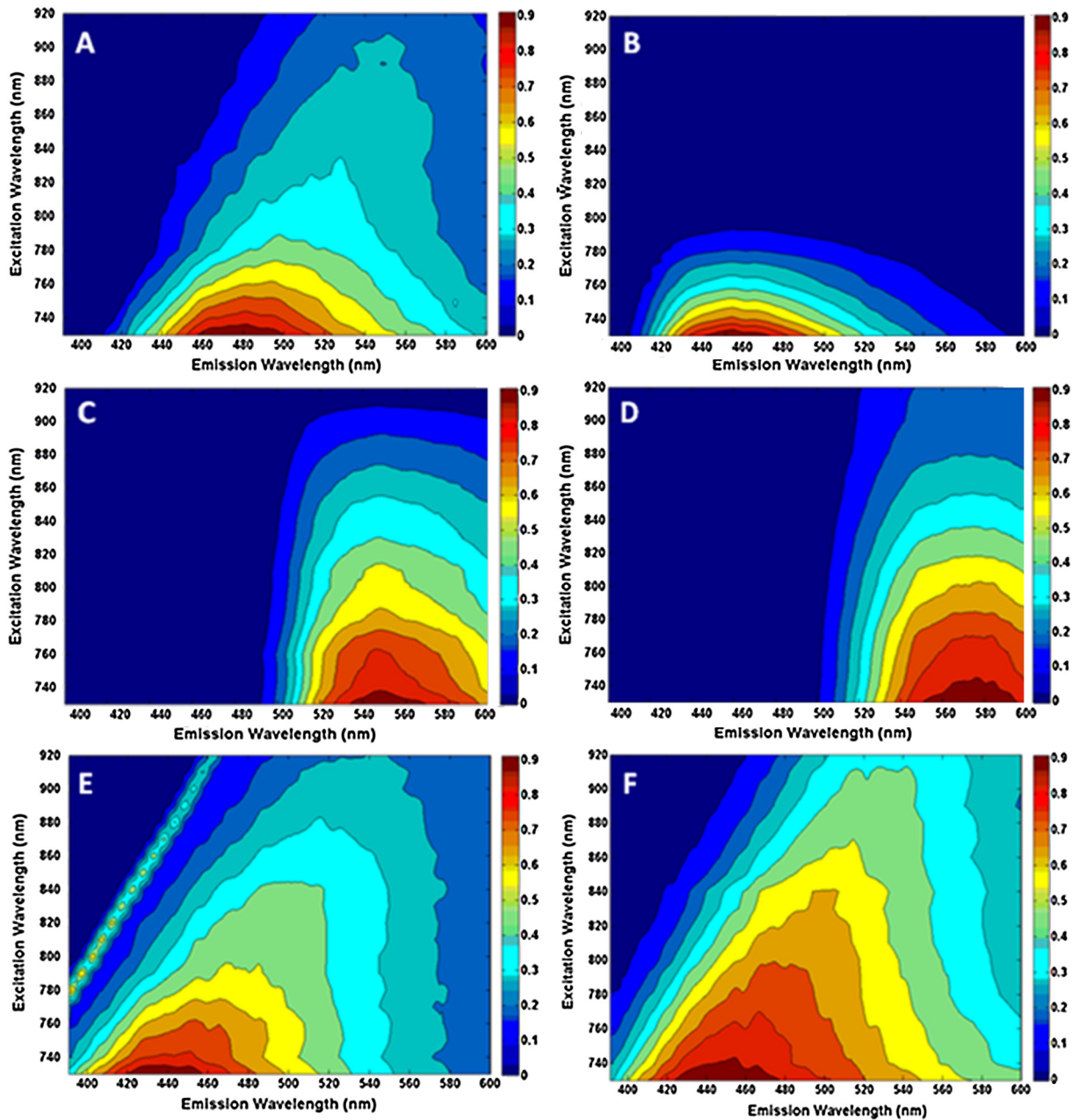


Fig. 2 Two-Photon EEM of endogenous fluorophores of human skin. (a) Keratin, (b) NADH, (c) FAD, (d) melanin, (e) collagen, (f) elastin (excitation wavelength: 730 to 920 nm, excitation power: 20 mw, exposure time: 3 s, ROI: 100 \times 100 μm^2).

To acquire accurate two-photon EEM, two sets of calibrations were completed including excitation path and emission path calibrations. In the excitation path, excitation power after the objective was calibrated to maintain a constant power for various excitation wavelengths. In the emission path, we completed wavelength calibration for the spectrometer using a Hg(Ar) calibration lamp (HG-1, Ocean Optics, Dunedin, FL) and the system (wavelength dependent) response calibration for the CCD detector and all the optical components in the emission beam path and inside the spectrometer using a NIST certified tungsten lamp (RS-10A-1, Gamma Scientific, San Diego, CA). The standard tungsten lamp was coupled to an integration sphere, which was then placed with its exit port aligned with the objective lens. The standard light then went through the whole emission path including the objective, the grating as well as other optical components and reached the CCD detector. The standard lamp spectrum supplied by the manufacture was then divided by the measured spectrum by the CCD to generate a calibration curve. The experimental tissue spectra were calibrated by multiplying with this calibration curve.

3 Results and Discussion

3.1 EEM of Extracted Endogenous Fluorophores

To help the analysis of the EEM of skin tissue, we performed a comprehensive study of the two-photon EEM of extracted endogenous fluorophores in skin tissue, including NADH, FAD, keratin, melanin, elastin, and collagen. Figure 2 shows the two-photon EEMs of the six endogenous fluorophores measured. NADH, FAD, keratin, elastin, and collagen samples were measured in the original condition (either dry powder or solution) from purchase. Melanin is measured in the 1 mg/mL NH_4OH solution because its fluorescence is too weak for measurement when it is in the solid form. There is no measurable TPF signal from NH_4OH solution, so no data processing was needed to separate contributions from melanin and NH_4OH . Excitation wavelength was tuned from 730 to 920 nm in 10-nm steps. In Fig. 2(a) to 2(d) are the main fluorophores in the cell-rich epidermis layer, and Fig. 2(e) and 2(f) are the fluorophores in the fiber-rich dermis layer. Due to the limited tunable wavelength range of our laser, we did not observe the full excitation-emission maxima from the EEMs. The keratin EEM in Fig. 2(a) suggests that its excitation-emission maximum will occur at an excitation wavelength shorter than 730 nm and the emission wavelength close to 480 nm. Reference 13 measured the TPF

emission spectra of keratin at a couple of different excitation wavelengths. Our EEM covered more excitation wavelengths and for those overlapping excitation wavelengths, our results are consistent with Ref. 13. For example, the excitation-emission pair of (760 nm, 485 nm) and (860 nm, 525 nm) we observed matched with their results of two pairs located at (760 nm, 475 ± 5 nm) and (860 nm, 515 ± 5 nm).¹³ Here the first number in parentheses is a given excitation wavelength, whereas the second number is the wavelength of corresponding emission spectrum maximum intensity position. These are characteristics of individual emission spectra, which are different from the excitation-emission maximum pair of the whole EEM plot in the literature.

Figure 2(b) shows the EEM of NADH. We observed an excitation-emission pair at (730 nm, 460 nm), which matches with the (730 nm, 465 nm) pair in Ref. 14. The excitation-emission pairs in Fig. 2(c) to 2(f) (EEMs for FAD, melanin, collagen, and elastin, respectively) were also matched to certain extent with the reported results.^{10,14,15} These excitation-emission pairs are summarized in Table 1. Because of the distinct EEM pattern of different fluorophores, it is helpful to use these fluorophore signatures to characterize the physiologic/biologic composition of skin tissue from the measured EEMs.

3.2 EEM of Human Skin Tissue Ex Vivo

The following experiment was performed on a piece of fresh normal skin (~ 2 -mm thick, $\sim 1 \times 1$ cm² area) excised from the temple area. The bulk tissue without sectioning was used directly for EEM measurements within 1 hour after excision. Using the optical sectioning capability of the multi-modality system, five distinct layers as revealed by the TPF/SHG imaging were measured at different depths from stratum corneum to the dermis. All EEMs were acquired from the whole FOV of the correlated images.

TPF imaging channel is represented by the green pseudocolor and SHG imaging channel is in red. As shown in Fig. 3, imaging depths of the four sublayers in the epidermis are: 10, 20, 30, and 40 μm , respectively. The sublayer with an imaging depth of 60 μm is in the dermis compartment. FOV for all images is $100 \times 100 \mu\text{m}^2$ and the scale bar in the figures represents 20 μm^2 . All Images were taken under the excitation wavelength of 790 nm and the excitation power of 30 mW. All the images shown in Fig. 3 are averaged over 50 frames of raw images. As seen in Fig. 3(a), stratum corneum cells have large size. The EEM excitation-emission pair located at

Table 1 Comparison of excitation-emission pairs of reported results and our measurement results.

Fluorophore	Measurement results (nm)	Reported results (nm)
Keratin	(760, 485), (860, 525)	(760, 475 ± 5), (860, 515 ± 5)
NADH	(730, 460)	(730, 465)
FAD	(730, 550), (900, 543)	(730, 545), (900, 540)
Melanin	(800, 579)	(800, 565)
Collagen	(750, 458), (770, 475), (850, 510)	(750, 461.9 ± 0.2), (770, 472.5 ± 0.2), (850, 503.0 ± 0.2)
Elastin	(750, 454), (770, 472), (850, 508)	(750, 457.9 ± 0.4), (770, 465.5 ± 0.4), (850, 503.3 ± 0.5)

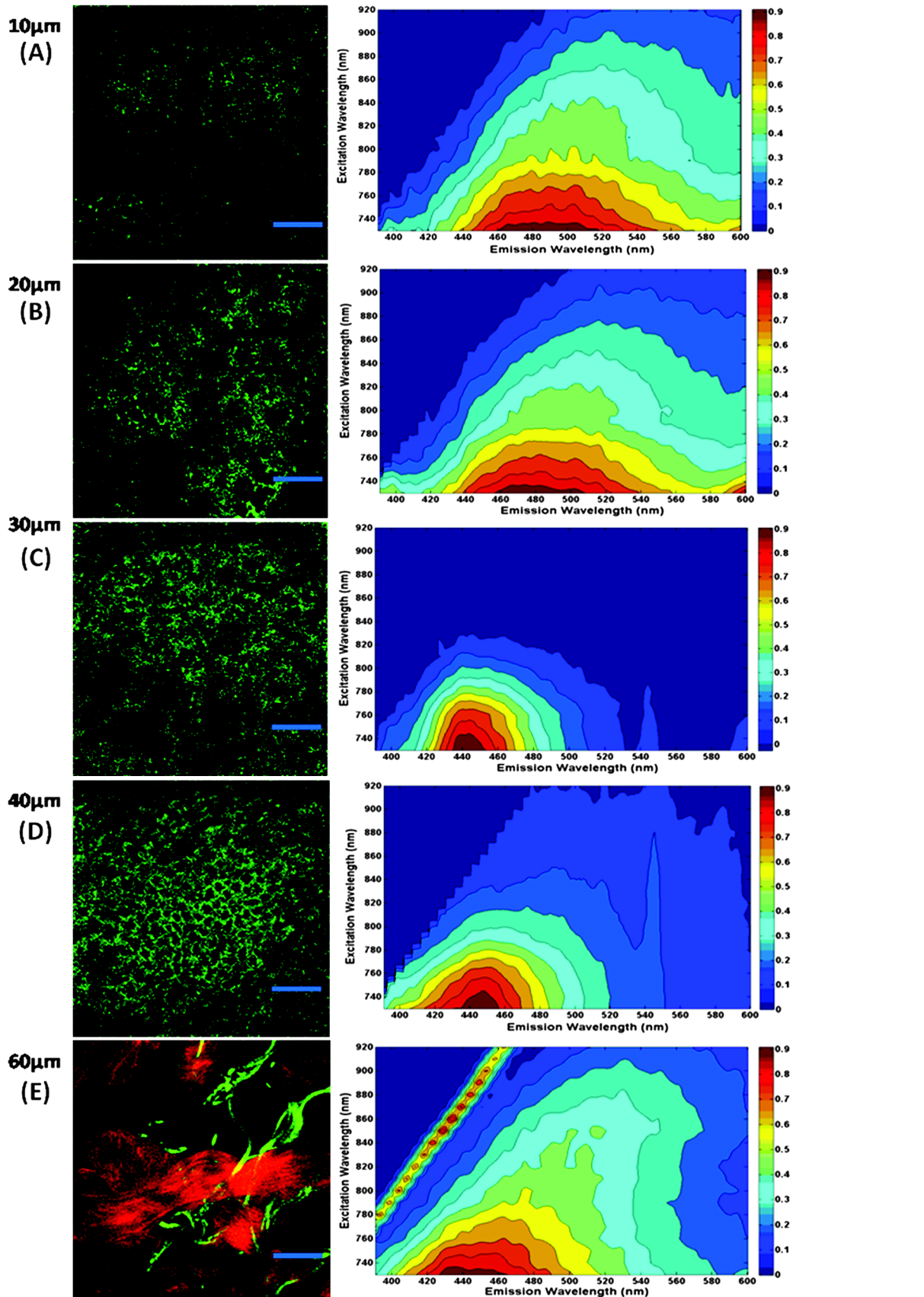


Fig. 3 Image-guided nonlinear EEM of normal human temple skin. Left column shows the pseudocolor image (TPF: green, SHG: red). Right column shows related EEM. Imaging depths include 10, 20, 30, 40, and 60 μm (imaging FOV: $100 \times 100 \mu\text{m}^2$, 50 frames averaged, scale bar: 20 μm , excitation power: 30 mW, excitation wavelength: 790 nm. EEM measurement excitation wavelength: 730–920 nm, exposure time: 2 s, ROI: $100 \times 100 \mu\text{m}^2$).

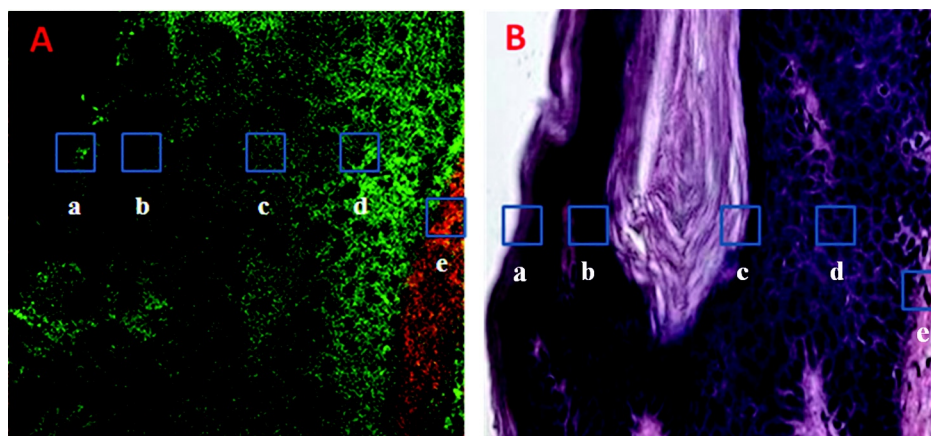


Fig. 4 Cross section images of human skin tissue with SK. (a) Combined image of TPF and SHG channels by pseudocolor (TPF: green, SHG: red). (b) Histology image with H&E staining (imaging FOV: $200 \times 200 \mu\text{m}^2$, Blue square: $20 \times 20 \mu\text{m}^2$).

(730 nm, 470 nm) is close to that of purified keratin as in our purified fluorophore measurement (730 nm, 480 nm). As we imaged deeper, the number of cells increased, whereas the size of the cells decreased. EEMs for the first two sub-layers [Fig. 3(a) and 3(b)] indicate that most of the TPF signals in these layers come from keratin, which mainly exists at and near the surface of skin. For the third and fourth sub-layers [Fig. 3(c) and 3(d)], the stratum spinosum and stratum basale, EEMs have the pattern and excitation emission pairs resembling that of pure NADH as shown in Fig. 2(b). It indicates that most of the TPF signal in these layers originates from NADH. NADH is significantly involved in redox reactions for metabolism; hence these EEMs show that cells are more active in stratum spinosum and stratum basale layers [Fig. 3(c) and 3(d)], which matches with the point of view of skin biology. Because cells in epidermis originate from stratum basale layer and keep proliferating and migrating to the top layers, the cells at a deeper layer are more active for metabolism. In Fig. 3(e), image and EEM data have been obtained for one layer in the dermis compartment. SHG channel was added and optimized for this layer for image-guidance purpose. The array of narrow peaks [along a diagonal line started at (780 nm, 390 nm)] in the EEM plot comprises SHG peaks with each emission peak located at exactly one-half of the excitation wavelength, respectively. The SHG signal originates from collagen fiber in the dermis layer. The peaks with much broader bandwidth represent TPF signal. TPF part of this EEM has a similar major excitation-emission pair of (730 nm, 450 nm) and overall pattern similar to both purified elastin and purified collagen. However, on the image, we see well-distinguished red and green bundles. The red bundles represent SHG signals that can only come from collagen fibers. Therefore, these large red colored bundles are collagen fibers for sure. They are pure red color without any green color component, indicating that collagen does not have significant fluorescence in this case (no TPF signal), otherwise they would appear yellowish. Therefore, the measured TPF spectral signals must come mostly from elastin. Indeed the image shows pure green smaller fibers that must be elastic fibers because of the lack of red color components and they are the dominant source of TPF spectral signals. SHG intensity in this EEM plot was attenuated 20 times so that the contour details of SHG and TPF signal can be displayed on a single plot. The SHG/TPF ratio for purified collagen is different from that of

collagen fibers in skin tissue, which may be due to that the purification process has changed the structures of collagen.

As an example of characterizing skin diseases, we investigated a seborrheic keratosis (SK) tissue sample from the shoulder region of a subject and compared with the results from normal skin. SK tissue usually has unique histologic characteristics, such as basal cells mixed with squamous cells and keratin-filled invaginations of the epithelium. As shown in Fig. 4, a slice of human shoulder SK skin is imaged with a FOV of $200 \times 200 \mu\text{m}^2$ for both two-photon images (TPF, SHG) and the histology image. This is a cross-section view including epidermis and dermis compartments. Figure 4(a) shows the overlay image of TPF and SHG channels (TPF in green, SHG in red), and Fig. 4(b) shows the matching H&E stained histology image to the best extent.

EEMs are acquired from five small areas (ROI) on this cross section as indicated by the blue squares ($20 \times 20 \mu\text{m}^2$) in Fig. 4. The EEMs are shown in Fig. 5 in the same order. In Fig. 5(a), the EEM has a similar pattern and excitation-emission pair as that of pure keratin sample. It is related to the blue square (a) in Fig. 4(a) and 4(b), where keratin structure can be observed clearly in the histological image. In both Fig. 5(b) and 5(d), the EEMs resemble that of pure NADH, which shows agreement with the cellular structures as highlighted by the blue square (b) and (d) in Fig. 4(a) and 4(b).

In Fig. 5(c), EEM seems to be a mixture of signals originating from various structures. The contour pattern and excitation-emission pairs below excitation of 760 nm (black dotted line) are similar to pure keratin, while EEM above 760 nm shows similarity with that of purified FAD sample in terms of the upright oriented EEM pattern and similar major excitation-emission-pairs for individual emission spectra, for example the pairs at (820 nm, 540 nm), (880 nm, 538 nm), and (900 nm, 535 nm) for the tissue are similar to the pairs at (820 nm, 548 nm), (880 nm, 542 nm), and (900 nm, 540 nm) for the FAD sample. This spectral characteristic matches with the image signal in the blue square (c) on Fig. 4(b), which includes both keratin and cellular structures in it. This analysis shows the advantage of EEM compared with single emission spectrum or excitation spectrum, because this tissue characteristic cannot be fully revealed using only one excitation wavelength or one emission wavelength. More importantly, the EEM reveals the fact that keratin structure has intruded into the middle sublayers of the epidermis part of the SK lesion. This result matches with the biologic characteristics of SK tissues, demonstrating the capability and

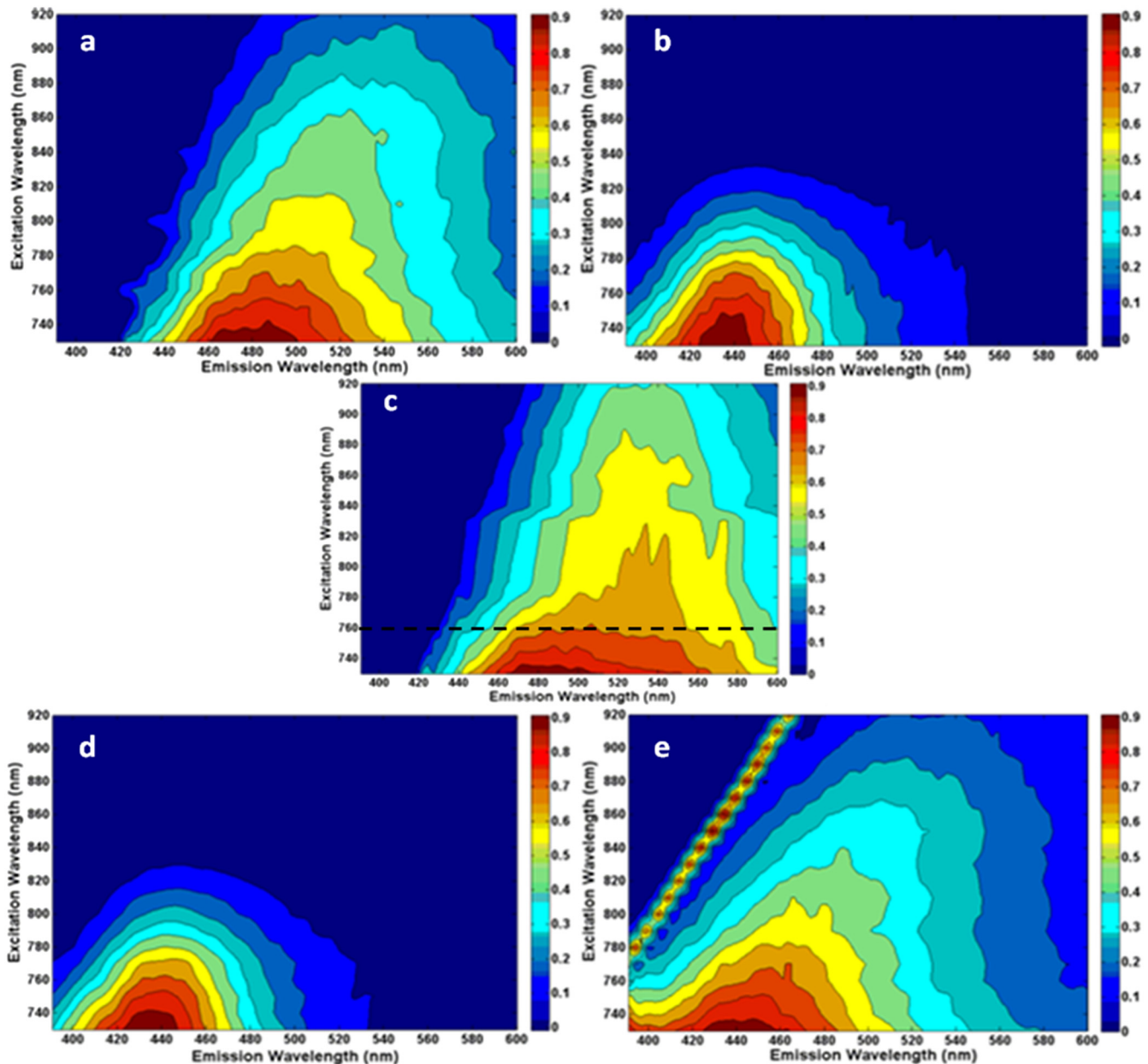


Fig. 5 EEM for human skin tissue with SK. (a)–(e) are measured from the corresponding blue square areas in Fig. 4 (excitation wavelength: 730 to 920 nm; excitation power: 30 mW, exposure time: 2 s, ROI: $20 \times 20 \mu\text{m}^2$).

great potential of applying the image-guided EEM for diagnosis of skin diseases. Figure 5(e) shows EEM for the last blue square (e) in Fig. 4(a) and 4(b), which is located in the dermis layer mainly containing fiber structures. The array of narrow peaks [along a diagonal line started at (780 nm, 390 nm)] is related to SHG peaks from collagen. The TPF spectra have a contour pattern similar to both purified elastin and purified collagen, whereas the image in Fig. 4(a), box (e) showed red color for the majority of pixels and yellow color for many other pixels nested within the red pixels. (The green pixels near the upper-left corner appear more likely to be cellular components, not collagen/elastic fibers.) This suggests that in this region of this SK lesion, collagen has great contributions to the TPF signals, different from normal dermal skin where elastin is the dominant TPF signal source. These differences deserve further investigations.

Comparing the results from normal skin tissue with that from SK, EEMs show different characteristics at different layers and show reasonable agreement with the biochemical characteristics of both tissue types. These results suggest the possibility of applying imaging-guided nonlinear EEM for skin disease diagnosis.

4 Conclusions

We presented a nonlinear EEM spectroscopy system with multimodality imaging guidance. The system was designed to optimize the imaging and spectroscopy performance in terms of imaging speed, resolution, and emission collection efficiency. Preliminary experiments on purified skin fluorophores as well as fresh normal and diseased skin tissues were carried out. With the depth-resolving capability, it revealed information in distinct skin layers inside the epidermis and dermis

compartments of bulk human skin tissue samples. Those EEMs show reasonable agreement with the tissue biologic characteristics observed by both the multiphoton imaging and the histology images. In the stratum corneum and upper epidermis (up to 20 μm in depth) of normal skin, the cells have large sizes and the TPF fluorescence originates from keratin. In the lower epidermis, cells are smaller and the TPF fluorescence is dominated by NADH contributions. We also further confirmed previous findings that in the dermis of normal skin, SHG signals originate from collagen, and that TPF are dominated by elastin components. It has also revealed interesting differences between normal skin and SK tissues. The depth resolved EEM measurements demonstrated the fact that keratin structure has intruded into the middle sublayers of the epidermis part of the SK lesion. These results suggest that the imaging guided TPF EEM spectroscopy provides useful information for the development of multiphoton clinical devices for skin disease diagnosis.

Acknowledgments

This work was funded by the Canadian Dermatology Foundation, the Natural Sciences and Engineering Research Council of Canada, the VGH and UBC Hospital Foundation In It for Life Fund, the BC Hydro Employees Community Services Fund, and the BC Cancer Agency. A.M.D.L. acknowledges the Michael Smith Foundation for Health Research (MSFHR) and the Canadian Institutes of Health Research Skin Research Training Centre (CIHR-SRTC) for postdoctoral fellowship support. H.W. acknowledges CIHR-SRTC for doctoral fellowship support.

References

1. W. R. Zipfel, R. M. Williams, and W. W. Webb, "Nonlinear magic: multiphoton microscopy in the biosciences," *Nat. Biotechnol.* **21**(11), 1369–1377 (2003).
2. J. Paoli et al., "Multiphoton laser scanning microscopy on non-melanoma skin cancer: morphologic features for future non-invasive diagnosis," *J. Invest. Derm.* **128**(5), 1248–1255 (2008).
3. J. Paoli, M. Smedh, and M. B. Ericson, "Multiphoton laser scanning microscopy: a novel diagnostic method for superficial skin cancers," *Semin. Cutan. Med. Surg.* **28**(3), 190–195 (2009).
4. R. Cicchi et al., "multidimensional non-linear imaging of basal cell carcinoma," *Opt. Express* **15**(16), 10135–10148 (2007).
5. Y. Wu and J. Y. Qu, "Two-photon autofluorescence spectroscopy and second-harmonic generation of epithelial tissue," *Opt. Lett.* **30**(22), 3045–3047 (2005).
6. L. H. Laiho et al., "Two-photon 3-D mapping of ex vivo human skin endogenous fluorescence species based on fluorescence emission spectra," *J. Biomed. Opt.* **10**(2), 024016 (2005).
7. S. Zhuo et al., "The layered-resolved microstructure and spectroscopy of mouse oral mucosa using multiphoton microscopy," *Phys. Med. Biol.* **52**(16), 4967–4980 (2007).
8. W. Zheng et al., "Autofluorescence of epithelial tissue: single-photon versus two-photon excitation," *J. Biomed. Opt.* **13**(5), 054010 (2008).
9. R. S. DaCosta, H. Andersson, and B. C. Wilson, "Molecular fluorescence excitation-emission matrices relevant to tissue spectroscopy," *Photochem. Photobiol.* **78**(4), 384–392 (2003).
10. J. Chen et al., "Spectroscopic characterization and microscopic imaging of extracted and in situ cutaneous collagen and elastic tissue components under two-photon excitation," *Skin. Res. Tech.* **15**(4), 418–426 (2009).
11. A. M. D. Lee et al., "In vivo video rate multiphoton microscopy imaging of human skin," *Opt. Lett.* **36**(15), 2865–2867 (2011).
12. M. J. Sanderson, "Acquisition of multiple real-time images for laser scanning microscopy," *Microscopy Anal.* **18**(4), 17–23 (2004).
13. A. M. Pena et al., "Spectroscopic analysis of keratin endogenous signal for skin multiphoton microscopy," *Opt. Express* **13**(16), 6268–6274 (2005).
14. S. Huang, A. A. Heikal, and W. W. Webb, "Two-photon fluorescence spectroscopy and microscopy of NADP(H) and flavoprotein," *Biophys. J.* **82**(5), 2811–2825(2002).
15. K. Teuchner et al., "Fluorescence studies of melanin by stepwise two-photon femtosecondlaser excitation," *J. Fluorescence.* **10**(3), 275–281 (2000).